Macromolecules

pubs.acs.org/Macromolecules Article

Strengthening the Intrachain Interconnection of Polymers by the Naphthalene Diimide–Pyrene Complementary Interactions

Hau-Ren Yang, Yen-Yu Chen, Han-Sheng Sun, Shih-Huang Tung, Shou-Ling Huang, Po-Chia Huang, Jey-Jau Lee, and Yu-Ying Lai*

Cite This: *Macromolecules* 2021, 54, 7282–7290 Read Online

ACCESS | Metrics & More | Article Recommendations | Supporting Information

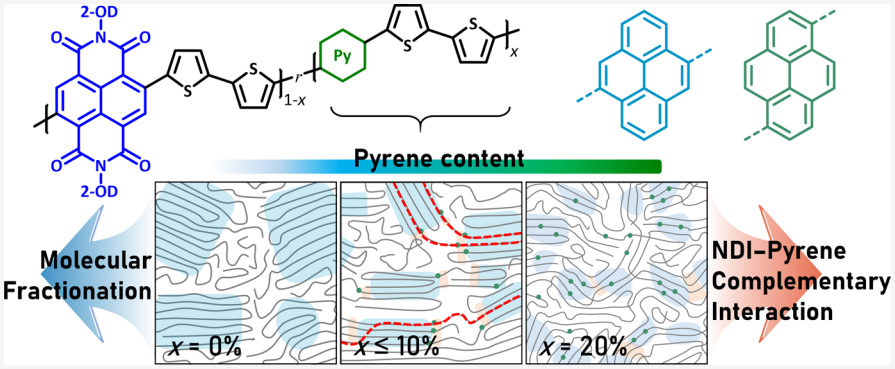

ABSTRACT: Two types of pyrenes are incorporated randomly into P(NDI2OD-T2). For the resultant polymers, the growth in the pyrene quantity results in the reduction of π-order. The decrease in π-order does not inevitably depreciate the organic field-effect transistor (OFET) mobility. A competitive mechanism between molecular fractionation and naphthalene diimide (NDI)–pyrene interactions is proposed. For moderate pyrene incorporation, molecular fractionation is dominant. Form I crystallites are fragmented, increasing the rigid amorphous fraction (RAF) regions. As for high pyrene content, the NDI–pyrene interactions take the lead, facilitating the establishment of a form II polymorph. The RAF can strengthen the interconnection among polymer crystallites. Overall, this work demonstrates a novel approach to intensifying the intrachain interconnection among polymers by the donor–acceptor (*i.e.*, NDI–pyrene) complementary interactions, offering pathways for efficient charge transporting in OFETs.

1. INTRODUCTION

For conjugated polymers, extensive π-order, being associated with high crystallinity, was conventionally considered the most significant parameter for realizing decent charge-transport mobility in organic field-effect transistors (OFETs).[1−9] This perspective has been challenged by numerous studies which point out that sufficient interconnection can preserve or even boost the charge mobility.[10−16] For instance, our previous work reveals that when NDIBu acts as an incorporator for P(NDI2OD-T2) (**P**, Figure 1a), the π-order of **P** is disturbed, being accompanied by the development of sporadic π-stacking.[17] The electron mobility could be considerably improved by the presence of sporadic π-stacking, substantiating that π-order is not compulsory. Selection of NDIBu is based on our earlier theoretical work which sheds light on the stacking principles for organic semiconductors, suggesting that the molecular shape plays the most crucial role in building long-range π-stacking.[18] Therefore, fractional substitution of butyl group for 2-octyldodecyl in **P** results in two different molecular figures, transforming oriented π-order into sporadic π-stacking. It can also be interpreted by molecular fractionation, stating that exclusion of segments containing hetero-units from crystallites is thermodyamically favored.[19]

On the other hand, it has been demonstrated that stable π-stacks can be established between naphthalene diimide (NDI) and pyrene.[20−23] In terms of molecular shape, pyrene resembles NDI. With regard to electronic properties, density functional theory (DFT) calculations at the ωB97XD/6-311g** level of theory indicate that the conjugated plane of NDI is electron deficient while that of pyrene is electron rich[24] (Figure 1b). It is envisioned that the resemblance in the molecular shape in conjunction with their complementary electronic properties is responsible for the strong affinity between NDI and pyrene, facilitating the formation of π-stacks. The NDI–pyrene complementary interactions intrigue us to

Received: February 9, 2021
Revised: June 9, 2021
Published: July 14, 2021

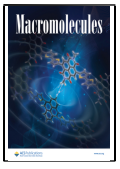

https://doi.org/10.1021/acs.macromol.1c00308
Macromolecules 2021, 54, 7282–7290

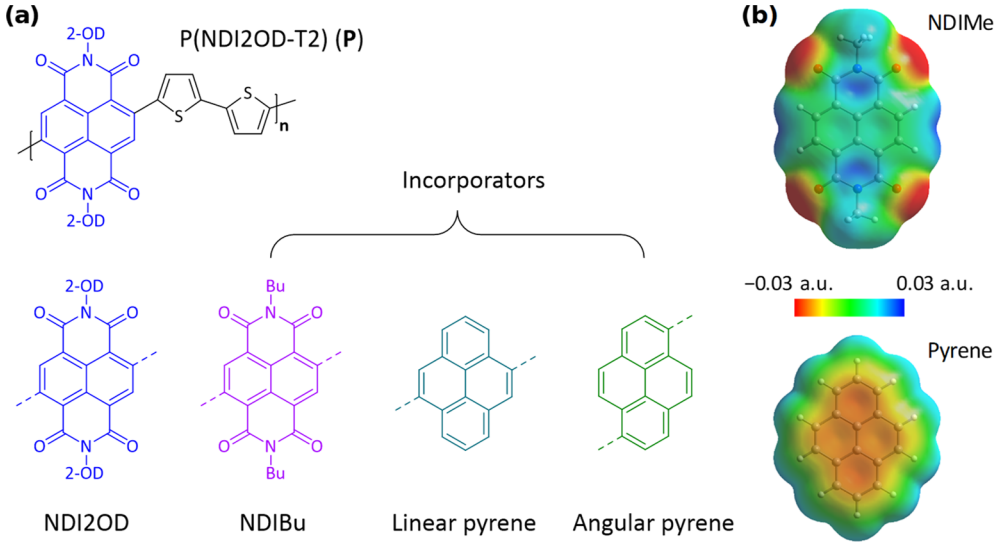

Figure 1. (a) Chemical structures of **P**, NDI2OD, NDIBu, and pyrenes. 2-OD: 2-octyldodecyl; Bu: *n*-butyl; linear pyrene: linkage at the 4,9 positions; angular pyrene: linkage at the 1,6 positions. (b) Electron density of NDIMe and pyrene mapped along the electrostatic potential at the ωB97XD/6-311g** level of theory.

Scheme 1. Synthetic Route of P, L05−L20, and A05−A20

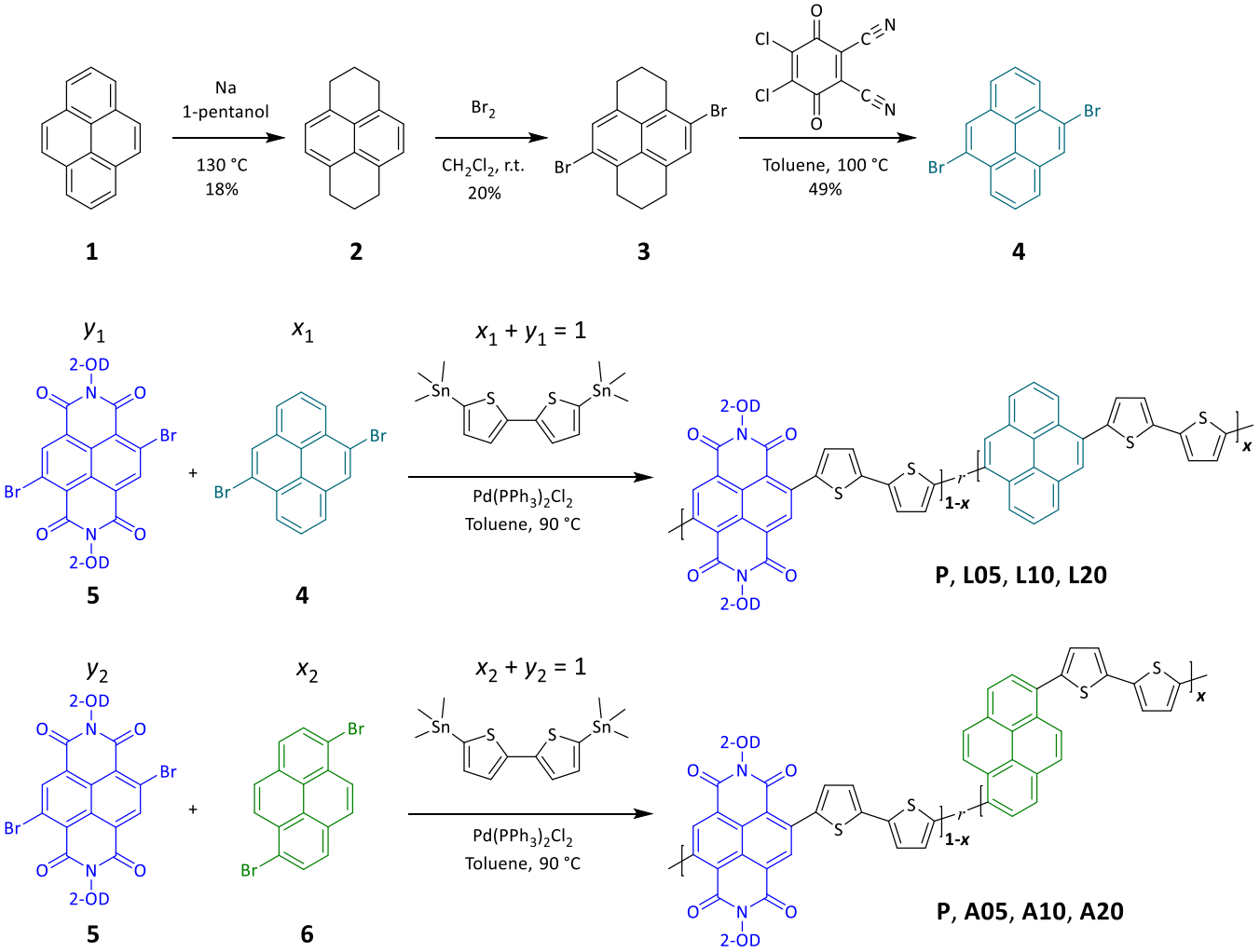

utilize pyrene as an incorporator for **P** to investigate the competition between molecular fractionation and NDI−pyrene interactions.

Hinging on the linkage, pyrenes could connect with bithiophenes at the 4,9 positions (linear pyrene) or 1,6 positions (angular pyrene) (Figure 1a), leading to linear

https://doi.org/10.1021/acs.macromol.1c00308
Macromolecules 2021, 54, 7282−7290

Table 1. Polymerization Results

polymers	feed ratio[a]	NMR ratio[b]	unaggregated/stacked[c]	ΔG[e] (kJ mol^{-1})	M_n[f] (kDa)	$Đ$[f]
P	100:0	100:0	56:44 (K_{eq} = 0.79)[d]	0.58	62	1.5
L05	95:5	93:7	17:83 (K_{eq} = 4.86)	−3.94	65	1.8
L10	90:10	87:13	16:84 (K_{eq} = 5.09)	−4.06	107	1.8
L20	80:20	81:19	18:82 (K_{eq} = 4.44)	−3.72	36	1.9
A05	95:5	93:7	26:74 (K_{eq} = 2.88)	−2.63	63	1.9
A10	90:10	88:12	18:82 (K_{eq} = 4.69)	−3.86	32	2.2
A20	80:20	82:18	18:82 (K_{eq} = 4.69)	−3.86	26	2.1

[a]Feed molar ratio of NDI to pyrene. [b]Molar ratio of NDI to pyrene in each polymer determined by ^{1}H NMR spectroscopy. [c]Molar ratio of unaggregated polymer chains to stacked polymer chains determined by ^{1}H NMR spectroscopy. [d]Equilibrium constant. [e]Change in Gibbs free energy, $\Delta G = -RT \ln(K_{eq})$, where R is the gas constant and T = 300 K. [f]Number-average molecular weight and dispersity determined by high-temperature gel permeation chromatography at 160 °C with 1,2,4-trichlorobenzene as an eluent.

polymers (**L**'s) or angular polymers (**A**'s). The fraction of pyrene in **P** was adjusted to afford numerous random copolymers with various amounts of pyrene moiety in the polymer chain. Through comparison of the results from ^{1}H NMR spectroscopy, UV−vis spectroscopy, differential scanning calorimetry (DSC), atomic force microscopy (AFM), and grazing-incidence X-ray scattering (GIXS), it is deduced that the polymer aggregation in solution and the thin-film morphology are affected largely by the presence of pyrene in the polymer scaffold. The variation in mobility for the polymers determined in OFETs is elucidated with the aid of microstructural alternation.

2. RESULTS AND DISCUSSION

Discussion starts with materials preparation, followed by characterization in the electronic properties, morphology, and thermal properties. Microstructure analysis is achieved with the assistance of GIXS. In the end, OFET results are illuminated by the help of morphological data along with DFT calculations.

2.1. Materials. The synthetic route[25−28] of the two series of polymers, **L**'s and **A**'s, is described in Scheme 1. Pyrene was hydrogenated through Birch reduction with sodium in 1-pentanol to afford 1,2,3,6,7,8-hexahydropyrene (**2**). Bromination of **2** by bromine furnished 4,9-dibromo-1,2,3,6,7,8-hexahydropyrene (**3**). 4,9-Dibromopyrene (**4**) was obtained by dehydrogenation of **3**. 2,6-Dibromonaphthalene-1,4,5,8-tetracarboxylic-*N*,*N*′-bis(2-octyldodecyl) diimide (**5**) was synthesized on the basis of a previous protocol.[17] 1,6-Dibromopyrene (**6**) was acquired from a commercial source. Random Stille copolymerization of **5** and **4** or **6** with pyrene fractions of 5, 10, and 20 mol % afforded two series of polymers, **L05**−**L20** or **A05**−**A20**, respectively. In the **L** series, pyrenes are linked with bithiophenes at the 4,9 positions, resulting in the formation of linear polymers. In the **A** series, connection takes place at the 1,6 positions, generating angular polymers. The number after **L** or **A** is the molar percentage of pyrene in feed, which is directly related to the stoichiometric coefficient x in Scheme 1.

The ^{1}H NMR spectra of all polymers are compared in Figure S1 (Supporting Information). According to the literature,[29,30] the chemical shift of 8.40−8.85 ppm stems from the aromatic protons of the NDI moiety, while pyrene's ^{1}H signals are in the range of 8.00−8.30 ppm. The molar ratio of NDI to pyrene in a polymer chain can be estimated by the integration value of absorption in ^{1}H NMR spectroscopy (Section S2, Polymerization, Supporting Information). As listed in Table 1, although there is a slight variation, all the estimated NMR ratios are close to the feed ratios, suggesting that incorporation of pyrene groups into **P** was achieved effectively.

Two sets of NDI aromatic chemical shifts were identified (Figure S1, Supporting Information). The experimental and theoretical studies performed by Neher and co-workers indicate that the more downshift signal derives from unaggregated polymer chains, while stacked polymer chains give rise to the more upshift absorption.[31] Adhering to their assignment, two sets of NDI absorptions observed in this study were also characterized as unaggregated and stacked polymer chains. NMR integration acquired by curve fitting revealed that unaggregated chains were dominant in **P**, whereas all polymers containing pyrene showed a preference for stacked chains (Table 1). Gibbs free energy difference (ΔG) was then estimated via the equilibrium constant (K_{eq}) between unaggregated and stacked chains, suggesting that in the **L**'s and **A**'s, the stacked chains were stabilized by about 2−4 kJ mol^{-1} in comparison with the unaggregated ones. It is very likely that the additional stabilization resulted from the NDI−pyrene interactions.

2.2. Electronic Properties. Photoemission spectroscopy[32] (Figure S3) and UV−vis absorption spectroscopy were performed to determine the highest occupied molecular orbital (HOMO) energies (E_H′s) and the optical band gap (E_g) of polymers. The lowest unoccupied molecular orbital (LUMO) energies (E_L′s) were then evaluated by $E_L = E_H + E_g$. The results are summarized in Table 2 and Figure S5 (Supporting Information). The E_g of **L**'s slightly rose with increasing linear pyrene moiety while that of **A**'s was invariant as the angular

Table 2. Electronic and Thermal Properties of P, L's, and A's

	electronic properties			thermal properties		
polymers	E_H[a] (eV)	E_g[b] (eV)	E_L[c] (eV)	T_d[d] (°C)	T_m[e] (°C)	ΔH (J g^{-1})
P	−5.80	1.46	−4.34	429	311	8.0[f]
L05	−5.76	1.46	−4.30	435	317	8.2[f]
L10	−5.74	1.46	−4.28	429	314	8.6[f]
L20	−5.71	1.51	−4.20	425	355	9.7[g]
A05	−5.68	1.45	−4.23	437	315	8.3[f]
A10	−5.67	1.45	−4.22	436	314	8.9[f]
A20	−5.60	1.45	−4.15	431	333	10.2[g]

[a]HOMO energy in thin film. [b]Thin-film optical band gap. [c]Estimated LUMO energy by $E_L = E_H + E_g$. [d]Decomposition temperature at 5% weight loss by thermogravimetric analysis. [e]Melting temperature. [f]Enthalpy of fusion of form I polymorph. [g]Enthalpy of fusion of form II polymorph.

https://doi.org/10.1021/acs.macromol.1c00308
Macromolecules 2021, 54, 7282−7290

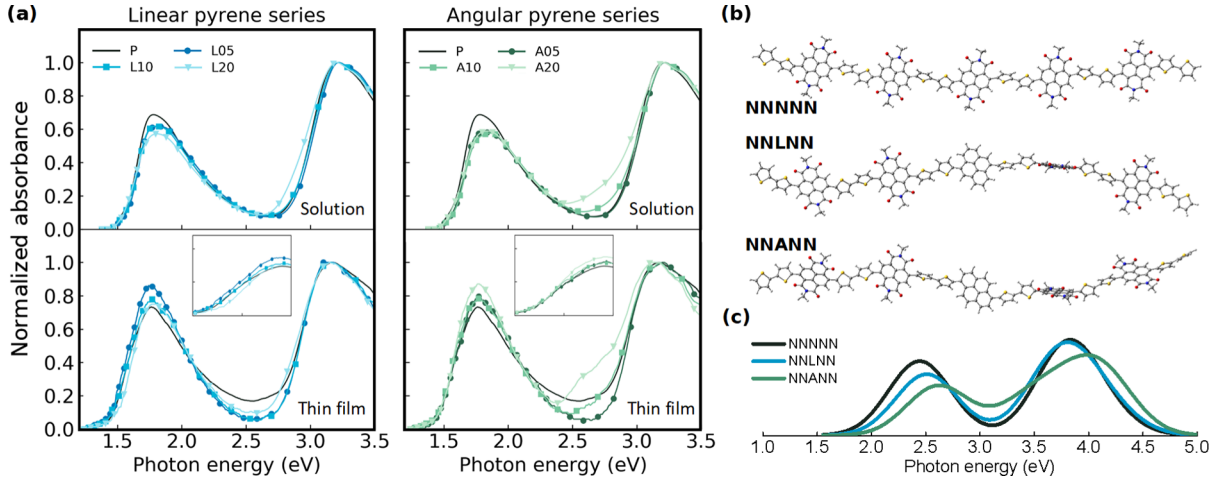

Figure 2. (a) UV−vis absorption spectra of all polymers in chloroform solution and thin film state. The spectra are normalized to the $\pi-\pi^*$ transition. The insets show magnified regions of the onset of ICT bands. (b) DFT-optimized structures of oligomers **NNNNN**, **NNLNN**, and **NNANN** represent **P**, **L**'s, and **A**'s, respectively. Gray: carbon. Yellow: sulfur. Red: oxygen. Blue: nitrogen. Light gray: hydrogen. (c) TD-DFT-simulated transition energies for the oligomers in (b), broadened in energy by σ = 400 meV.

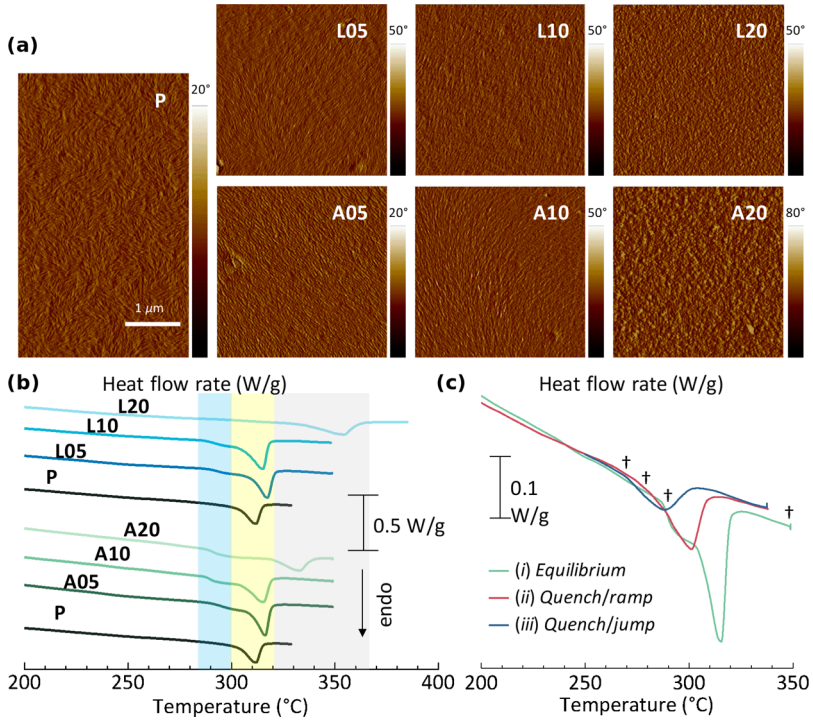

Figure 3. (a) AFM phase images. The color level indices are set to start from the zero phase. (b) DSC heating thermograms of **P**, **L**'s, and **A**'s. (c) DSC heating thermograms of **A10** in different thermal histories. The dagger symbols indicate the corresponding temperatures in temperature-dependent GIXS (Figure 4c).

pyrene content was increased. The replacement of NDI units with pyrenes in the polymer backbone raised both the E_H and E_L because of the electron-donating properties of pyrene.

The absorption spectra of all polymers in chloroform and in a thin film are described in Figure 2a. Two absorption bands at ≈1.55 and ≈3.20 eV were found for all polymers, and no apparent shift in the absorption maximum, especially in the thin film, was observed. It was noted that enhanced absorption at ≈2.7 eV was present in pyrene-rich polymers, such as **L20** and **A20**. To gain insights into the UV−vis absorption spectra, time-dependent DFT (TD-DFT) calculations were performed by using a long-range corrected functional CAM-B3LYP with the 6-31G** basis set.[33,34] Three pentamers, **NNNNN**, **NNLNN**, and **NNANN**, were designed to represent the polymers, **P**, **L**'s, and **A**'s, respectively (Figure 2b). In the nomenclature, **N**, **L**, and **A** denote NDI, linear pyrene, and angular pyrene. The computational results indicate that the intramolecular charge transfer (ICT)[35,36] from bithiophenes to NDIs is the dominant contribution in the absorption at ≈1.55 eV, and the absorption band at ≈3.20 eV mainly comes from $\pi-\pi^*$ transitions (Figure S6, Supporting Information). Moreover, additional $\pi-\pi^*$ transitions of pyrene coupling with bithiophene functionality are estimated theoretically. These transitions might be responsible for the experimental

https://doi.org/10.1021/acs.macromol.1c00308
Macromolecules 2021, 54, 7282−7290

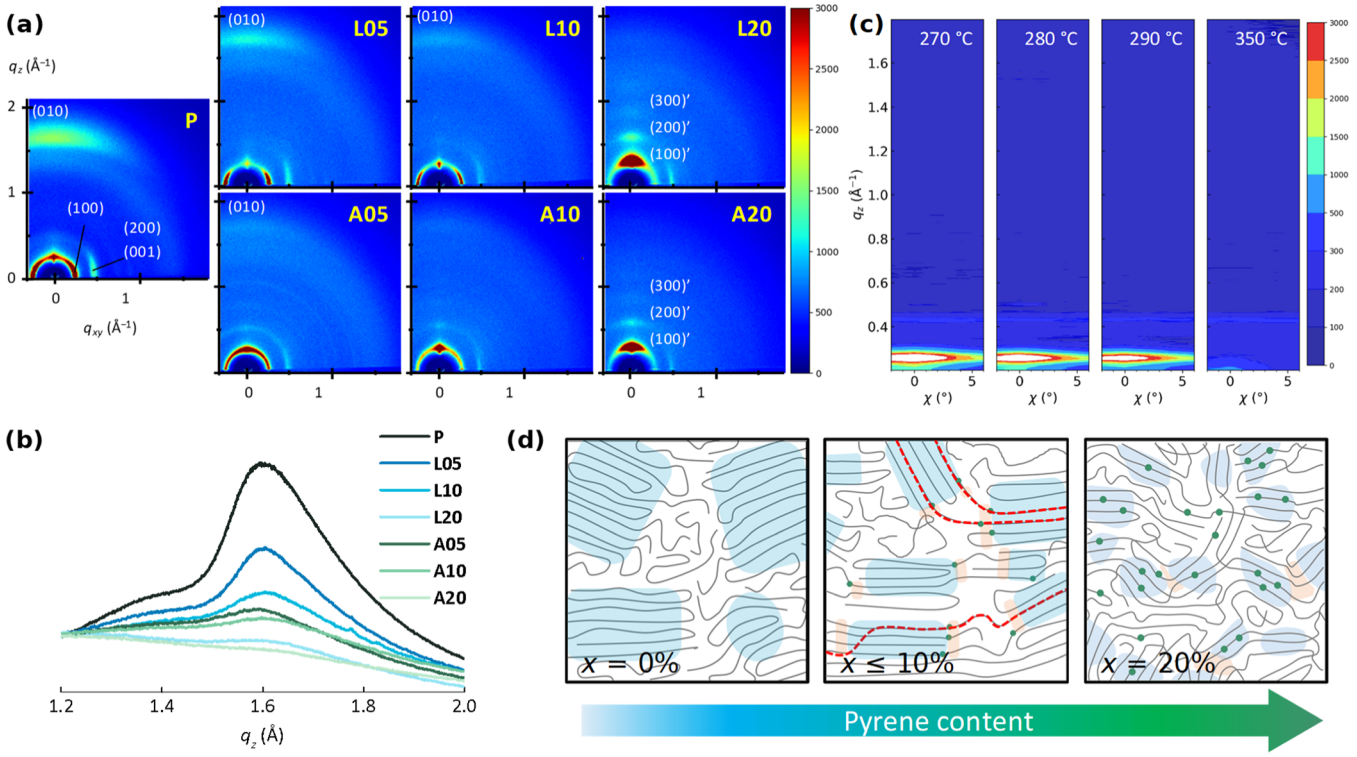

Figure 4. (a) Diffraction patterns given by GIXS. (b) Change in the out-of-plane π-stacking signature in different pyrene contents. (c) Temperature-dependent GIXS images of **A10**. χ: The azimuthal angle. (d) Effect of the pyrene incorporation on thin-film microstructure. Green nodes, blue-shaded regions, and orange-shaded regions represent pyrene units, π-order, and the RAF, respectively.

observation of enhanced absorption at ≈2.7 eV in pyrene-rich polymers. The simulated absorption spectra shown in Figure 2c suggest that a hypsochromic shift of the ICT band is expected as the introduction of pyrene into **P**, which was not yet detected experimentally, in a thin film in particular. The discrepancy suggests that interchain or intrachain J-aggregation might take place in the thin film.[37,38] The bathochromic shift being typical of J-aggregation might compensate for the hypsochromic shift developing out of pyrene.

2.3. Morphology and Thermal Properties. The thin-film surface morphology was investigated by AFM. (Large-scale height and phase images are included in Figure S7, Supporting Information.) Transition from fibers to globules was observed as the increase in the pyrene unit in the polymer (Figure 3a). Comparison of **L20** and **A20** images revealed that globules deriving from angular pyrene were more perceptible than those from linear pyrenes. Two-dimensional fast Fourier transformation of height images (Figure S7c) was carried out to extract the average dimensions of aggregates,[39] quantifying the transition.

The thermal decomposition temperatures (T_d's) of all polymers in Table 2 determined by thermogravimetric analysis (Section S8, Supporting Information) exceeded 400 °C, authenticating the following thermal-related characterizations. Endothermic thermograms determined by DSC are depicted in Figure 3b, and the enthalpy of fusion (ΔH) is included in Table 2. As there is an increase in the pyrene group in the polymer chain, the rise of melting temperature (T_m) was observed. Moreover, the T_m variation suggested that there were two primary thermal transitions which might be responsible for the morphology transition observed in AFM. One was T = 300−322 °C (the yellow-shaded region) and the other was T = 322−365 °C (the gray-shaded region), which was readily identified in **L20** and **A20**. It is envisaged that the two transitions relate to two polymorphic forms, which is supported by GIXS in a section below. The lower temperature region was derived from form I, whereas form II was dominant in the higher one. The similar T_m of polymers under moderate pyrene content ($x \leq 10\%$) might suggest that form I preserved the crystalline structure of **P**. In contrast, the distinguishing T_m of polymers in high-level incorporation (x = 20%) indicated that the occurrence of form II might be associated with the NDI−pyrene interactions.

Intriguingly, a shoulder area (T = 280−300 °C, the blue-shaded region) prior to the melting of form I was perceptible for polymers with moderate pyrene incorporation ($x \leq 10\%$). The shoulder might be considered as a thermal transition of a certain amorphous fraction of the polymer. A semicrystalline polymer could contain two kinds of amorphous regions, that is, mobile amorphous fraction (MAF) where the polymer chains have superior segmental mobility[40,41] and rigid amorphous fraction (RAF) where the polymer chains are constrained near the boundary of crystallites.[42−44] It has been reported that the glass-transition temperature of **P** is in the range of 74−100 °C,[45−47] which should derive from the MAF. The RAF ought to yield another glass transition, which is characterized to be the shoulder signal herein. Each endothermic DSC curve of **L05**, **L10**, **A05**, and **A10** in the vicinity of the melting peak is fitted with a combination of two functions (Section S8, Supporting Information). The first is to describe a heat flow curve of **P** and the second defines a sigmoid curve delineating the glass transition of RAF. The proportion of RAF can be quantified by the latter one. Optimized parameters (Table S2, Supporting Information) suggest that the glass transition of RAF can be augmented by increasing pyrene contents.

https://doi.org/10.1021/acs.macromol.1c00308
Macromolecules 2021, 54, 7282−7290

In order to further investigate the possibility of RAF formation, **A10** was submitted to different thermal treatments and the results are presented in Figure 3c. The green curve, (i) equilibrium, indicates that **A10** was annealed for 30 min at a temperature right below the temperature of crystallization and then heated at a scan rate of 10 °C min^{-1}. The red curve, (ii) quench/ramp, denotes that the melt of **A10** was quenched by liquid nitrogen to afford a supercooled solid, which was then heated at a scan rate of 10 °C min^{-1}. In the blue curve, (iii) quench/jump, the supercooled solid was directly heated to 250 °C and then heated gradually at a scan rate of 10 °C min^{-1}. The thermal treatments from (i) to (iii) can be interpreted as gradual suppression of crystallization. Both the melting peak of form I crystallites (T_m = 315 °C) and the shoulder peak were detected in the green curve. However, the melting peak of form I crystallites was suppressed in the red and blue curves, pointing out that polymers in the supercooled solid did not have sufficient amount of time to crystallize. Hence, the RAF was also suppressed. The results suggest that establishment of thermal equilibrium is essential for the development of the shoulder peak. Overall, the shoulder exhibited characteristics of the RAF.[48]

Given that the shoulder peak resulted from the RAF, in addition to form I and form II, the RAF was also taken into consideration. The ΔH of form I remained virtually constant (Table 2), while the RAF developed steadily as the pyrene incorporation (indicated by the change of heat capacity of a polymer during the course of glass transition, W_s in Table S2, Supporting Information). This might be associated with the statement that after the introduction of pyrene, crystallites of form I became fragmentary, thus generating more RAF regions.

2.4. Microstructure Analysis. A typical face-on polymorph with strong out-of-plane π-stacking ($q \approx 1.6$ $Å^{-1}$) arising out of form I crystallites was detected in **P** by GIXS (Figures 4a and S10), being consistent with the literature.[49,50] The face-on π-stacking signal (010) was weakened gradually as the increase in linear pyrene in the polymer (Figure 4b). In contrast, the diminution of the π-stacking signal was evident for the polymers with angular pyrene. It is expected that linear and angular pyrenes would result in linear and angular backbone architectures, respectively. The angular architecture with more irregular backbone symmetry might much discourage the building of π-order, leading to the swift drop in the π-stacking.[51] Similar conclusions can be drawn from the variation of coherence length estimated from one-dimensional diffractograms using the Scherrer's equation.[52,53] For the face-on polymorph, the coherence lengths of π-stacking ($L_{c,\pi}$) and lamellar stacking ($L_{c,L}$) both decreased as the incorporation of pyrene groups (Table S3, Supporting Information). The decline was much more pronounced for angular pyrene. The coherence length of polymer backbone ($L_{c,B}$) was not adversely affected by the presence of pyrene (Table S3, Supporting Information). Instead, all the polymers comprising pyrene showed comparable or higher $L_{c,B}$ than pristine **P**, being an indication of preserving or even improving intrachain interconnection among crystallites. DSC results suggested that **L20** and **A20** exhibited another polymorph. Figure 4a revealed that out-of-plane diffractions with high orders (100)′, (200)′, and (300)′ were identified merely for **L20** and **A20**. The corresponding d-spacing was ≈24 Å, being consistent with the lamellar stacking stemming from side-chain interdigitation. The results are in harmony with the formation of form II deduced from DSC. Moreover, the plots of (010) intensity against the azimuthal angle χ are included in Section 9, Supporting Information.[54−60] The variation in the (010) signal and the emergence of (100)′, (200)′, and (300)′ signals along the q_z suggest that the orientation of polymer crystallites might change from face-on to edge-on to a certain degree. In consideration of the diminution of $L_{c,\pi}$, the virtually constant ΔH of form I polymorph implied the formation of more small-sized form I crystallites under moderate pyrene content ($x \leq$ 10%). In other words, crystallites of form I became fragmentary, generating more RAF regions.

The shoulder area observed in DSC was further investigated by temperature-dependent GIXS. As illustrated in Figure 4c, variation in the diffraction pattern of **A10** in the selected area was insignificant from 270 to 290 °C. Nevertheless, when the temperature (350 °C) exceeded T_m, the signal vanished virtually. The results indicated that the thermal transition in the shoulder area should be ascribed to the amorphous fraction rather than the crystalline one. The identity of the shoulder to be RAF is supported by temperature-dependent GIXS, as well (see Section S9 of the Supporting Information for more examples).

The stacking principle reported earlier by our group states that integration of hetero-units into a crystallite would heighten the total free energy. Provided that exclusion of hetero-units from crystallites is favored, the corresponding progression is entitled as the molecular fractionation.[19] On the other hand, the NDI−pyrene interactions could encourage the interference of pyrene in the crystallites of **P**, likely constraining the crystallite development. The tug of war between the molecular fractionation and NDI−pyrene interactions might be present in the polymers. In the event of moderate pyrene incorporation ($x \leq$ 10%), even though form I crystallites turned to be fragmenting, they were still detected, pointing out that the molecular fractionation was governing. Meanwhile, the rejected pyrene segments outside of the form I crystallites could dock at the NDI units to gain the NDI−pyrene interactions. The glass transition of RAF thus developed with increasing pyrene ratio (see Table S2 and Figure S9). On the contrary, the NDI−pyrene interactions might prevail in the polymers of high-level incorporation of pyrene (x = 20%), leading to the establishment of the polymorphic form II. The growth of the RAF and the increasing amount of fragmentary crystallites indicated that the interconnection among polymer crystallites was established by our approach. Overall, the morphological variation brought by the pyrene unit is illustrated in Figure 4d.

2.5. OFET Characteristics. The microstructural regulation by incorporating pyrene units into **P** was examined electrically by measuring the field-effect mobility of electrons (μ_e) in the saturation regime with bottom-gate/top-contact OFETs. Details of device fabrication and measurement are included in Section S10, Supporting Information. The average and maximal μ_e's for all the polymers are depicted in Figure 5. For **L**'s, the variation in the maximal μ_e seems to be consistent with the average μ_e. The correlation between the maximal and average mobilities is yet not significant for **A**'s. **L**'s reached a maximum of 0.134 cm^2 V^{-1} s^{-1} at 5% linear pyrene loading while a maximum of 0.152 cm^2 V^{-1} s^{-1}, being 3.5 times greater than the archetypal **P**, was achieved by **A10** for **A**'s.

Electronic coupling between the NDI and pyrene was investigated by DFT calculations[61−66] (Section S11, Supporting Information), indicating that the intermolecular electronic coupling would be deteriorated by the presence of either linear

https://doi.org/10.1021/acs.macromol.1c00308
Macromolecules 2021, 54, 7282−7290

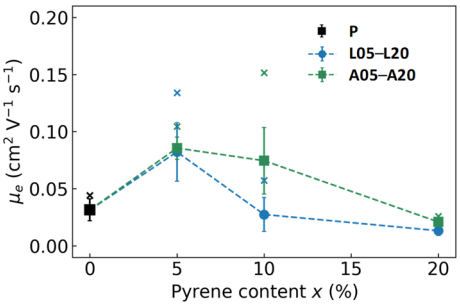

Figure 5. Dependence of electron mobility on the pyrene content. Box symbols for the average mobility; cross symbols for the maximal mobility; error bars: the standard deviation (dashed lines are guides to the eye).

or angular pyrene. Given that the results are applicable to polymers, it is envisaged that the pyrene incorporation is detrimental to the interchain charge transport of polymers. Moreover, DFT calculations (Figure 1b) also suggest that NDI is a π-electron-deficient chromophore, while pyrene is π-electron rich. The growth of pyrene units in **P** is expected to intensify the energetic disorder in the polymer chain, depreciating the intrachain charge transport efficiency. With regard to the electronic properties, μ_e should be reduced notably by the introduction of pyrene into **P**. Nevertheless, the above presumption does not fit with our OFET data.

DSC indicates that the pyrene incorporation could increase the RAF among polymers. The RAF can improve the interconnection among polymer crystallites, encouraging the charge transport.[67−69] GIXS suggests that the orientation of polymer crystallites might change as the increase in the pyrene fraction. The morphological benefit brought by pyrene could counteract their intrinsic electronic disadvantage, accounting for preservation or even improvement of the μ_e subsequent to the introduction of pyrene to **P**.

Our previous study demonstrates that when NDIBu acts as an incorporator for **P**, periodic π-stacking of **P** is transformed to sporadic π-stacking, which is coined as π-interconnection therein. The μ_e could be considerably improved by the presence of sporadic π-stacking. In the present study, as discussed, preservation or improvement of μ_e primarily results from the RAF, which is regarded as intrachain interconnection. Overall, our works suggest that either interchain or intrachain interconnection could be established by incorporating a hetero-unit into a polymer. The preference strongly depends on the structure and functionality of the hetero-unit.

3. CONCLUSIONS

On account of the NDI−pyrene complementary interactions, pyrene is chosen as an incorporator for **P**. Spectroscopic, microscopic, and X-ray measurements along with thermal characterization reveal that the incorporation of pyrene has significant effects on polymer aggregation in the solution and morphology in the thin film. The rise in the pyrene quantity in **P** would result in the reduction of π-order. Competition between the molecular fractionation and the NDI−pyrene interactions is proposed. For moderate pyrene incorporation, the molecular fractionation is dominant, giving rise to fragmentary form I crystallites and generating more RAF regions. As for high pyrene content, the NDI−pyrene interactions take the lead, promoting the building of form II polymorph. It is envisioned that the RAF can enhance the interconnection among polymer crystallites, facilitating the charge transport. Moreover, the results emphasize again that the π-order is not a necessity for accomplishing decent OFET mobility. In a nutshell, our work demonstrates a novel approach to strengthening the intrachain interconnection among polymers by the donor−acceptor (*i.e.*, NDI−pyrene) complementary interactions, providing pathways for efficient charge transporting.

■ ASSOCIATED CONTENT

Supporting Information

The Supporting Information is available free of charge at https://pubs.acs.org/doi/10.1021/acs.macromol.1c00308.

Results for polymerization, synthesis, GPC, photoemission spectroscopy and energy level diagram, quantum chemical computation, AFM, thermal properties, GIXS, OFET fabrication and measurements, and NMR spectra (PDF)

■ AUTHOR INFORMATION

Corresponding Author

Yu-Ying Lai − *Institute of Polymer Science and Engineering, National Taiwan University, Taipei 10617, Taiwan;* orcid.org/0000-0002-1921-6923; Email: yuyinglai@ntu.edu.tw

Authors

Hau-Ren Yang − *Institute of Polymer Science and Engineering, National Taiwan University, Taipei 10617, Taiwan*

Yen-Yu Chen − *Institute of Polymer Science and Engineering, National Taiwan University, Taipei 10617, Taiwan*

Han-Sheng Sun − *Institute of Polymer Science and Engineering, National Taiwan University, Taipei 10617, Taiwan*

Shih-Huang Tung − *Institute of Polymer Science and Engineering, National Taiwan University, Taipei 10617, Taiwan;* orcid.org/0000-0002-6787-4955

Shou-Ling Huang − *Department of Chemistry, National Taiwan University, Taipei 10617, Taiwan*

Po-Chia Huang − *National Synchrotron Radiation Research Center, Hsinchu 30076, Taiwan;* orcid.org/0000-0002-7007-5206

Jey-Jau Lee − *National Synchrotron Radiation Research Center, Hsinchu 30076, Taiwan*

Complete contact information is available at: https://pubs.acs.org/10.1021/acs.macromol.1c00308

Notes

The authors declare no competing financial interest.

■ ACKNOWLEDGMENTS

We acknowledge the support of this work by the Ministry of Science and Technology, Taiwan and National Taiwan University (NTU-110L7822, higher Education Sprout Project). We thank the X-ray diffraction and absorption facilities provided by the National Synchrotron Radiation Research Center, Taiwan (beamline 17A). We express our gratitude to the Center for Emerging Material and Advanced Devices, National Taiwan University, for providing the thermal evaporator. We thank the National Center for High-performance Computing (NCHC) and the NTU Computer and Information Networking Center for providing computational

and storage resources. We gratefully thank Huang, Shou-Ling for the assistance in NMR experiments of the Instrumentation Center at NTU, which is supported by the Ministry of Science and Technology, Taiwan. We appreciate the group of professor Yen-Ju Cheng for the assistance in OFET and GPC measurements. We acknowledge the group of professor Yi-Tsu Chan for help in GPC measurement.

REFERENCES

(1) Klimovich, I. V.; Leshanskaya, L. I.; Troyanov, S. I.; Anokhin, D. V.; Novikov, D. V.; Piryazev, A. A.; Ivanov, D. A.; Dremova, N. N.; Troshin, P. A. Design of indigo derivatives as environment-friendly organic semiconductors for sustainable organic electronics. *J. Mater. Chem. C* **2014**, *2*, 7621−7631.
(2) Botiz, I.; Stingelin, N. Influence of Molecular Conformations and Microstructure on the Optoelectronic Properties of Conjugated Polymers. *Materials* **2014**, *7*, 2273−2300.
(3) Wang, H.; Xu, Y.; Yu, X.; Xing, R.; Liu, J.; Han, Y. Structure and Morphology Control in Thin Films of Conjugated Polymers for an Improved Charge Transport. *Polymers* **2013**, *5*, 1272−1324.
(4) Back, J. Y.; Yu, H.; Song, I.; Kang, I.; Ahn, H.; Shin, T. J.; Kwon, S.-K.; Oh, J. H.; Kim, Y.-H. Investigation of Structure−Property Relationships in Diketopyrrolopyrrole-Based Polymer Semiconductors via Side-Chain Engineering. *Chem. Mater.* **2015**, *27*, 1732−1739.
(5) Tsao, H. N.; Cho, D. M.; Park, I.; Hansen, M. R.; Mavrinskiy, A.; Yoon, D. Y.; Graf, R.; Pisula, W.; Spiess, H. W.; Müllen, K. Ultrahigh Mobility in Polymer Field-Effect Transistors by Design. *J. Am. Chem. Soc.* **2011**, *133*, 2605−2612.
(6) Di Pietro, R.; Erdmann, T.; Carpenter, J. H.; Wang, N.; Shivhare, R. R.; Formanek, P.; Heintze, C.; Voit, B.; Neher, D.; Ade, H.; Kiriy, A. Synthesis of High-Crystallinity DPP Polymers with Balanced Electron and Hole Mobility. *Chem. Mater.* **2017**, *29*, 10220−10232.
(7) Yang, J.; Zhao, Z.; Geng, H.; Cheng, C.; Chen, J.; Sun, Y.; Shi, L.; Yi, Y.; Shuai, Z.; Guo, Y.; Wang, S.; Liu, Y. Isoindigo-Based Polymers with Small Effective Masses for High-Mobility Ambipolar Field-Effect Transistors. *Adv. Mater.* **2017**, *29*, 1702115.
(8) Sirringhaus, H. 25th Anniversary Article: Organic Field-Effect Transistors: The Path Beyond Amorphous Silicon. *Adv. Mater.* **2014**, *26*, 1319−1335.
(9) Usta, H.; Facchetti, A.; Marks, T. J. n-Channel Semiconductor Materials Design for Organic Complementary Circuits. *Acc. Chem. Res.* **2011**, *44*, 501−510.
(10) Kim, M.; Park, W.-T.; Ryu, S. U.; Son, S. Y.; Lee, J.; Shin, T. J.; Noh, Y.-Y.; Park, T. Improving the Electrical Connection of n-Type Conjugated Polymers through Fluorine-Induced Robust Aggregation. *Chem. Mater.* **2019**, *31*, 4864−4872.
(11) Son, S. Y.; Kim, Y.; Lee, J.; Lee, G.-Y.; Park, W.-T.; Noh, Y.-Y.; Park, C. E.; Park, T. High-Field-Effect Mobility of Low-Crystallinity Conjugated Polymers with Localized Aggregates. *J. Am. Chem. Soc.* **2016**, *138*, 8096−8103.
(12) Noriega, R.; Rivnay, J.; Vandewal, K.; Koch, F. P. V.; Stingelin, N.; Smith, P.; Toney, M. F.; Salleo, A. A general relationship between disorder, aggregation and charge transport in conjugated polymers. *Nat. Mater.* **2013**, *12*, 1038−1044.
(13) Wang, S.; Fabiano, S.; Himmelberger, S.; Puzinas, S.; Crispin, X.; Salleo, A.; Berggren, M. Experimental evidence that short-range intermolecular aggregation is sufficient for efficient charge transport in conjugated polymers. *Proc. Natl. Acad. Sci. U.S.A.* **2015**, *112*, 10599.
(14) Noriega, R. Efficient Charge Transport in Disordered Conjugated Polymer Microstructures. *Macromol. Rapid Commun.* **2018**, *39*, 1800096.
(15) Gu, K.; Loo, Y. L. The Polymer Physics of Multiscale Charge Transport in Conjugated Systems. *J. Polym. Sci., Part B: Polym. Phys.* **2019**, *57*, 1559−1571.
(16) Kong, H.; Lee, D. H.; Seo, J.-I.; Oh, J.-Y.; Chung, D. S.; Park, J.-W.; Kwon, S.-K.; Lee, Y. S.; Park, C. E.; Shim, H.-K. A New Amorphous Semiconducting Polythiophene for High-Performance Organic Thin-Film Transistors. *ACS Appl. Mater. Interfaces* **2010**, *2*, 1100−1106.
(17) Yang, H. R.; Lai, Y. Y.; Lee, J. J. Further Examination of Interconnection in Conjugated Polymers for Organic Field-Effect Transistors. *Adv. Electron. Mater.* **2019**, *5*, 1900213.
(18) Lai, Y.-Y.; Huang, V.-H.; Lee, H.-T.; Yang, H.-R. Stacking Principles on π- and Lamellar Stacking for Organic Semiconductors Evaluated by Energy Decomposition Analysis. *ACS Omega* **2018**, *3*, 18656−18662.
(19) Gedde, U. W. *Polymer Physics*; Gedde, U. W., Ed.; Kluwer Academic Publishers: Dordrecht, 1999.
(20) Kumar, N. S. S.; Gujrati, M. D.; Wilson, J. N. Evidence of preferential π-stacking: a study of intermolecular and intramolecular charge transfer complexes. *Chem. Commun.* **2010**, *46*, 5464−5466.
(21) Gujrati, M. D.; Kumar, N. S. S.; Brown, A. S.; Captain, B.; Wilson, J. N. Luminescent Charge-Transfer Complexes: Tuning Emission in Binary Fluorophore Mixtures. *Langmuir* **2011**, *27*, 6554−6558.
(22) Greenland, B. W.; Burattini, S.; Hayes, W.; Colquhoun, H. M. Design, synthesis and computational modelling of aromatic tweezer-molecules as models for chain-folding polymer blends. *Tetrahedron* **2008**, *64*, 8346−8354.
(23) Burattini, S.; Greenland, B. W.; Merino, D. H.; Weng, W.; Seppala, J.; Colquhoun, H. M.; Hayes, W.; Mackay, M. E.; Hamley, I. W.; Rowan, S. J. A Healable Supramolecular Polymer Blend Based on Aromatic $\pi-\pi$ Stacking and Hydrogen-Bonding Interactions. *J. Am. Chem. Soc.* **2010**, *132*, 12051−12058.
(24) Yeh, M.-Y.; Lin, H.-C. Theoretical analysis of the intermolecular interactions in naphthalene diimide and pyrene complexes. *Phys. Chem. Chem. Phys.* **2014**, *16*, 24216−24222.
(25) Lee, J.; Park, J. Synthesis and Electroluminescence of Novel Pyrene-Fused Chromophores. *Org. Lett.* **2015**, *17*, 3960−3963.
(26) Gu, P.-Y.; Wang, Z.; Liu, G.; Yao, H.; Wang, Z.; Li, Y.; Zhu, J.; Li, S.; Zhang, Q. Synthesis, Full Characterization, and Field Effect Transistor Behavior of a Stable Pyrene-Fused N-Heteroacene with Twelve Linearly Annulated Six-Membered Rings. *Chem. Mater.* **2017**, *29*, 4172−4175.
(27) Liu, F.; Shen, X.; Wu, Y.; Bai, L.; Zhao, H.; Ba, X. Synthesis of ladder-type graphene ribbon oligomers from pyrene units. *Tetrahedron Lett.* **2016**, *57*, 4157−4161.
(28) Bheemireddy, S. R.; Ubaldo, P. C.; Finke, A. D.; Wang, L.; Plunkett, K. N. Contorted aromatics via a palladium-catalyzed cyclopentannulation strategy. *J. Mater. Chem. C* **2016**, *4*, 3963−3969.
(29) Yan, H.; Chen, Z.; Zheng, Y.; Newman, C.; Quinn, J. R.; Dötz, F.; Kastler, M.; Facchetti, A. A high-mobility electron-transporting polymer for printed transistors. *Nature* **2009**, *457*, 679−686.
(30) Kim, Y.; Long, D. X.; Lee, J.; Kim, G.; Shin, T. J.; Nam, K.-W.; Noh, Y.-Y.; Yang, C. A Balanced Face-On to Edge-On Texture Ratio in Naphthalene Diimide-Based Polymers with Hybrid Siloxane Chains Directs Highly Efficient Electron Transport. *Macromolecules* **2015**, *48*, 5179−5187.
(31) Steyrleuthner, R.; Schubert, M.; Howard, I.; Klaumünzer, B.; Schilling, K.; Chen, Z.; Saalfrank, P.; Laquai, F.; Facchetti, A.; Neher, D. Aggregation in a High-Mobility n-Type Low-Bandgap Copolymer with Implications on Semicrystalline Morphology. *J. Am. Chem. Soc.* **2012**, *134*, 18303−18317.
(32) Fallon, K. J.; Wijeyasinghe, N.; Manley, E. F.; Dimitrov, S. D.; Yousaf, S. A.; Ashraf, R. S.; Duffy, W.; Guilbert, A. A. Y.; Freeman, D. M. E.; Al-Hashimi, M.; Nelson, J.; Durrant, J. R.; Chen, L. X.; McCulloch, I.; Marks, T. J.; Clarke, T. M.; Anthopoulos, T. D.; Bronstein, H. Indolo-naphthyridine-6,13-dione Thiophene Building Block for Conjugated Polymer Electronics: Molecular Origin of Ultrahigh n-Type Mobility. *Chem. Mater.* **2016**, *28*, 8366−8378.
(33) Peach, M. J. G.; Cohen, A. J.; Tozer, D. J. Influence of Coulomb-attenuation on exchange−correlation functional quality. *Phys. Chem. Chem. Phys.* **2006**, *8*, 4543−4549.
(34) Adamo, C.; Jacquemin, D. The calculations of excited-state properties with Time-Dependent Density Functional Theory. *Chem. Soc. Rev.* **2013**, *42*, 845−856.

https://doi.org/10.1021/acs.macromol.1c00308
Macromolecules 2021, 54, 7282−7290

(35) Jespersen, K. G.; Beenken, W. J. D.; Zaushitsyn, Y.; Yartsev, A.; Andersson, M.; Pullerits, T.; Sundström, V. The electronic states of polyfluorene copolymers with alternating donor-acceptor units. *J. Chem. Phys.* **2004**, *121*, 12613−12617.
(36) Hassan, S. Z.; Cheon, H. J.; Choi, C.; Yoon, S.; Kang, M.; Cho, J.; Jang, Y. H.; Kwon, S.-K.; Chung, D. S.; Kim, Y.-H. Molecular Engineering of a Donor−Acceptor Polymer To Realize Single Band Absorption toward a Red-Selective Thin-Film Organic Photodiode. *ACS Appl. Mater. Interfaces* **2019**, *11*, 28106−28114.
(37) Spano, F. C.; Silva, C. H- and J-Aggregate Behavior in Polymeric Semiconductors. *Annu. Rev. Phys. Chem.* **2014**, *65*, 477−500.
(38) Brixner, T.; Hildner, R.; Köhler, J.; Lambert, C.; Würthner, F. Exciton Transport in Molecular Aggregates − From Natural Antennas to Synthetic Chromophore Systems. *Adv. Energy Mater.* **2017**, *7*, 1700236.
(39) Hsu, L.-C.; Kobayashi, S.; Isono, T.; Chiang, Y.-C.; Ree, B. J.; Satoh, T.; Chen, W.-C. Highly Stretchable Semiconducting Polymers for Field-Effect Transistors through Branched Soft−Hard−Soft Type Triblock Copolymers. *Macromolecules* **2020**, *53*, 7496−7510.
(40) Qian, Z.; Cao, Z.; Galuska, L.; Zhang, S.; Xu, J.; Gu, X. Glass Transition Phenomenon for Conjugated Polymers. *Macromol. Chem. Phys.* **2019**, *220*, 1900062.
(41) Xiao, M.; Sadhanala, A.; Abdi-Jalebi, M.; Thomas, T. H.; Ren, X.; Zhang, T.; Chen, H.; Carey, R. L.; Wang, Q.; Senanayak, S. P.; Jellett, C.; Onwubiko, A.; Moser, M.; Liao, H.; Yue, W.; McCulloch, I.; Nikolka, M.; Sirringhaus, H. Linking Glass-Transition Behavior to Photophysical and Charge Transport Properties of High-Mobility Conjugated Polymers. *Adv. Funct. Mater.* **2021**, *31*, 2007359.
(42) Wunderlich, B. Reversible crystallization and the rigid−amorphous phase in semicrystalline macromolecules. *Prog. Polym. Sci.* **2003**, *28*, 383−450.
(43) Di Lorenzo, M. L.; Righetti, M. C. Crystallization-induced formation of rigid amorphous fraction. *Polym. Cryst.* **2018**, *1*, No. e10023.
(44) Schick, C.; Androsch, R. The Origin of Annealing Peaks in Semicrystalline Polymers: Enthalpy Recovery or Melting? *Macromolecules* **2020**, *53*, 8751−8756.
(45) Schuettfort, T.; Huettner, S.; Lilliu, S.; Macdonald, J. E.; Thomsen, L.; McNeill, C. R. Surface and Bulk Structural Characterization of a High-Mobility Electron-Transporting Polymer. *Macromolecules* **2011**, *44*, 1530−1539.
(46) Sharma, A.; Pan, X.; Bjuggren, J. M.; Gedefaw, D.; Xu, X.; Kroon, R.; Wang, E.; Campbell, J. A.; Lewis, D. A.; Andersson, M. R. Probing the Relationship between Molecular Structures, Thermal Transitions, and Morphology in Polymer Semiconductors Using a Woven Glass-Mesh-Based DMTA Technique. *Chem. Mater.* **2019**, *31*, 6740−6749.
(47) Xie, R.; Weisen, A. R.; Lee, Y.; Aplan, M. A.; Fenton, A. M.; Masucci, A. E.; Kempe, F.; Sommer, M.; Pester, C. W.; Colby, R. H.; Gomez, E. D. Glass transition temperature from the chemical structure of conjugated polymers. *Nat. Commun.* **2020**, *11*, 893.
(48) Martín, J.; Stingelin, N.; Cangialosi, D. Direct Calorimetric Observation of the Rigid Amorphous Fraction in a Semiconducting Polymer. *J. Phys. Chem. Lett.* **2018**, *9*, 990−995.
(49) Rivnay, J.; Toney, M. F.; Zheng, Y.; Kauvar, I. V.; Chen, Z.; Wagner, V.; Facchetti, A.; Salleo, A. Unconventional Face-On Texture and Exceptional In-Plane Order of a High Mobility n-Type Polymer. *Adv. Mater.* **2010**, *22*, 4359−4363.
(50) Rivnay, J.; Noriega, R.; Kline, R. J.; Salleo, A.; Toney, M. F. Quantitative analysis of lattice disorder and crystallite size in organic semiconductor thin films. *Phys. Rev. B: Condens. Matter Mater. Phys.* **2011**, *84*, 045203.
(51) Steyrleuthner, R.; Di Pietro, R.; Collins, B. A.; Polzer, F.; Himmelberger, S.; Schubert, M.; Chen, Z.; Zhang, S.; Salleo, A.; Ade, H.; Facchetti, A.; Neher, D. The Role of Regioregularity, Crystallinity, and Chain Orientation on Electron Transport in a High-Mobility n-Type Copolymer. *J. Am. Chem. Soc.* **2014**, *136*, 4245−4256.
(52) Warren, B. E. *X-ray Diffraction*; Warren, B. E., Ed.; Dover Publications: New York, 1990.
(53) Smilgies, D.-M. Scherrer grain-size analysis adapted to grazing-incidence scattering with area detectors. *J. Appl. Crystallogr.* **2009**, *42*, 1030−1034.
(54) Baker, J. L.; Jimison, L. H.; Mannsfeld, S.; Volkman, S.; Yin, S.; Subramanian, V.; Salleo, A.; Alivisatos, A. P.; Toney, M. F. Quantification of Thin Film Crystallographic Orientation Using X-ray Diffraction with an Area Detector. *Langmuir* **2010**, *26*, 9146−9151.
(55) Johnston, D. E.; Yager, K. G.; Hlaing, H.; Lu, X.; Ocko, B. M.; Black, C. T. Nanostructured Surfaces Frustrate Polymer Semiconductor Molecular Orientation. *ACS Nano* **2014**, *8*, 243−249.
(56) Olla, T.; Ibraikulov, O. A.; Ferry, S.; Boyron, O.; Méry, S.; Heinrich, B.; Heiser, T.; Lévêque, P.; Leclerc, N. Benzothiadiazole Halogenation Impact in Conjugated Polymers, a Comprehensive Study. *Macromolecules* **2019**, *52*, 8006−8016.
(57) Page, K. A.; Kusoglu, A.; Stafford, C. M.; Kim, S.; Kline, R. J.; Weber, A. Z. Confinement-Driven Increase in Ionomer Thin-Film Modulus. *Nano Lett.* **2014**, *14*, 2299−2304.
(58) Rivnay, J.; Mannsfeld, S. C. B.; Miller, C. E.; Salleo, A.; Toney, M. F. Quantitative Determination of Organic Semiconductor Microstructure from the Molecular to Device Scale. *Chem. Rev.* **2012**, *112*, 5488−5519.
(59) Zhang, X.; Bronstein, H.; Kronemeijer, A. J.; Smith, J.; Kim, Y.; Kline, R. J.; Richter, L. J.; Anthopoulos, T. D.; Sirringhaus, H.; Song, K.; Heeney, M.; Zhang, W.; McCulloch, I.; DeLongchamp, D. M. Molecular origin of high field-effect mobility in an indacenodithiophene−benzothiadiazole copolymer. *Nat. Commun.* **2013**, *4*, 2238.
(60) Hammond, M. R.; Kline, R. J.; Herzing, A. A.; Richter, L. J.; Germack, D. S.; Ro, H.-W.; Soles, C. L.; Fischer, D. A.; Xu, T.; Yu, L.; Toney, M. F.; DeLongchamp, D. M. Molecular Order in High-Efficiency Polymer/Fullerene Bulk Heterojunction Solar Cells. *ACS Nano* **2011**, *5*, 8248−8257.
(61) *Practical Aspects of Computational Chemistry IV*; Leszczynski, J., Shukla, M. K., Eds.; Springer US: Boston, MA, 2016.
(62) Wu, T.-L.; Kuo, C.-H.; Lin, B.-C.; Tao, Y.-T.; Hsu, C.-P.; Liu, R.-S. Synthesis of planar dibenzo[de,op]bistetracene derivatives for organic field-effect transistor applications: substituent effect on crystal packing and charge transport property. *J. Mater. Chem. C* **2015**, *3*, 7583−7588.
(63) Ji, L.-F.; Fan, J.-X.; Zhang, S.-F.; Ren, A.-M. Theoretical investigations into the charge transfer properties of thiophene α-substituted naphthodithiophene diimides: excellent n-channel and ambipolar organic semiconductors. *Phys. Chem. Chem. Phys.* **2017**, *19*, 13978−13993.
(64) Wen, S.-H.; Li, A.; Song, J.; Deng, W.-Q.; Han, K.-L.; Goddard, W. A. First-Principles Investigation of Anistropic Hole Mobilities in Organic Semiconductors. *J. Phys. Chem. B* **2009**, *113*, 8813−8819.
(65) Valeev, E. F.; Coropceanu, V.; da Silva Filho, D. A.; Salman, S.; Brédas, J.-L. Effect of Electronic Polarization on Charge-Transport Parameters in Molecular Organic Semiconductors. *J. Am. Chem. Soc.* **2006**, *128*, 9882−9886.
(66) Li, H.; Brédas, J.-L. Developing molecular-level models for organic field-effect transistors. *Natl. Sci. Rev.* **2021**, *8*, 1−14.
(67) Fratini, S.; Nikolka, M.; Salleo, A.; Schweicher, G.; Sirringhaus, H. Charge transport in high-mobility conjugated polymers and molecular semiconductors. *Nat. Mater.* **2020**, *19*, 491−502.
(68) Noriega, R.; Salleo, A.; Spakowitz, A. J. Chain conformations dictate multiscale charge transport phenomena in disordered semiconducting polymers. *Proc. Natl. Acad. Sci. U.S.A.* **2013**, *110*, 16315.
(69) Gu, K.; Snyder, C. R.; Onorato, J.; Luscombe, C. K.; Bosse, A. W.; Loo, Y.-L. Assessing the Huang−Brown Description of Tie Chains for Charge Transport in Conjugated Polymers. *ACS Macro Lett.* **2018**, *7*, 1333−1338.

https://doi.org/10.1021/acs.macromol.1c00308
Macromolecules 2021, 54, 7282−7290